Korean J. Chem. Eng., 38(8), 1676-1685 (2021)
DOI: 10.1007/s11814-021-0799-z

pISSN: 0256-1115
eISSN: 1975-7220

Construction of OH sites within MIL-101(Cr)-NH_2 framework for enhanced CO_2 adsorption and CO_2/N_2 selectivity

The Ky Vo*,†, Pham Van Vu*, Van Cuong Nguyen*, and Jinsoo Kim,†**

*Department of Chemical Engineering, Industrial University of Ho Chi Minh City, 12 Nguyen Van Bao, Go Vap, Ho Chi Minh City, Vietnam
**Department of Chemical Engineering (Integrated Engineering), Kyung Hee University, 1732 Deogyeong-daero, Giheung-gu, Yongin-si, Gyeonggi-do 17104, Korea
(*Received 13 January 2021 • Revised 14 March 2021 • Accepted 4 April 2021*)

Abstract−The MIL-101(Cr)-NH_2 framework was effectively modified by 2,5-dihydroxyterephthalic acid ($(HO)_2BDC$) guest molecules to obtain $(HO)_2BDC$-incorporated MIL-101(Cr)-NH_2 adsorbent, namely $(HO)_2BDC$@CrN. The CO_2-temperature programmed-desorption (TPD) analysis indicated that the incorporation of $(HO)_2BDC$ into the MIL-101(Cr)-NH_2 framework generated new OH sites besides unsaturated Cr- metal sites and NH_2 sites. The formed OH sites improved CO_2 adsorption and separation on the prepared adsorbent. The highest CO_2 uptake capacity of ~3.58 mmol g^{-1} obtained over the novel $(HO)_2BDC$@CrN adsorbent was higher 40% than that of the parent MOF, and also surpasses that of other previously reported adsorbents, including activated carbon, nitrogen-doped hollow carbon, zeolite, ZIF-68, MOF-5, ZIF-8, UiO-66(Zr), and MIL-100(Cr). The highest ideal adsorbed solution theory (IAST) CO_2/N_2 selectivity of ~67 was obtained over the $(HO)_2BDC$@CrN adsorbent at 100 kPa. The achieved selectivity was six times greater than that of pure MIL-101(Cr)-NH_2. In addition, the synthesized $(HO)_2BDC$@CrN adsorbent displayed good regenerability after six consecutive adsorption-desorption cycles.

Keywords: CO_2 Adsorption, MIL-101(Cr)-NH_2, Dihydroxyterephthalic Acid, $(HO)_2BDC$@CrN, CO_2/N_2 Separation, CO_2-TPD

INTRODUCTION

Burning fossil fuels, including coal, natural gas, or oil, results in increased levels of carbon dioxide (CO_2) in the atmosphere, which has become one of the major environmental issues worldwide [1, 2,62]. CO_2 capture and separation employing novel materials, such as metal-organic framework (MOFs), has been proposed as the potential strategy to control the CO_2 emissions [20,30,31,76].

MOFs, a new class of porous compounds formed through pervasive coordination bonds between metal cations and organic ligands, are promising adsorbent materials [16,45,54,58,63]. Compared to traditional adsorbent materials, MOFs are distinguished by an ultrahigh surface area, large pore volume, and ordered pore structure with tunable pore size [27,38,60]. These characteristics enable their application in various fields, including gas adsorption and separation [5,53,55,59], catalysis [29,46], drug delivery [41], and sensing [12]. Numerous MOFs have been studied for CO_2 capture and separation. Previously reported materials include MOF-5, MOF-74(Mg), MIL-53(Al), HKUST-1, UiO-66(Zr), UiO-67(Zr), MIL-101(Cr), and MIL-101(Cr)-NH_2 [38,62]. Most of them exhibit considerably greater CO_2 uptake capacity than those displayed by conventional adsorbents such as zeolites or carbon materials [3,48, 71,77]. For effective CO_2 capture from flue gas, high CO_2 adsorption capacity and selectivity have become requisites for new MOFs. Many strategies have been developed to enhance the CO_2 adsorption ability and selectivity of these materials. Among them, the modification of MOFs by incorporation of unsaturated metal cation centers, metal doping, and chemical functionalization has been found to be effective [8,10,76]. For instance, Jeo et al. [25] reported that M-incorporated MOF-74(M) (M=Mg^{2+}, Ni^{2+}, or Co^{2+}) possessed tunable CO_2 adsorption properties. Additionally, Bae et al. [2] synthesized Li-containing MOFs by chemical reduction and cation exchange, resulting in a significant increase in the CO_2 adsorption capacity and CO_2/CH_4 selectivity. On the other hand, Zhou et al. [76] synthesized a novel bimetallic MIL-101(Cr, Mg), which exhibited a 40% increase of the CO_2 uptake capacity compared to MIL-101(Cr). However, several metal-doped MOFs were found to be moisture-sensitive, which considerably hinders their practical application, since water vapor is ubiquitous [13,76].

In recent years, incorporation of carbon materials into MOFs has attracted significant attention to improve the CO_2 adsorption ability and selectivity. For example, Zhou et al. [74] prepared GrO@MIL-101 and found that the material displayed noticeably higher CO_2 uptake capacity and CO_2/CH_4 selectivity than that of traditional adsorbents and other MOFs. Moreover, GO@Cu-BTC [22], GO@MIL-53(Cr) [73], and UiO-66/graphene [9] showed enhanced CO_2 adsorption capacity and selectivity. It is noteworthy that recently, pre- or post-modification strategies for incorporation of basic amine functionalities into MOFs have been utilized to further improve the CO_2 uptake capacity and selectivity. A series of amine-incorporated MOF adsorbents with enhanced selective CO_2 adsorption capacity have been reported. These include amine-decorated MIL-101(Cr)

†To whom correspondence should be addressed.
E-mail: votheky@iuh.edu.vn, jkim21@khu.ac.kr

[66], polyamine/MIL-101(Cr) [37], en-MIL-100(Cr), mmen-MIL-100(Cr) [8], ethylenediamine-incorporated MIL-101(Cr)-NH_2 [57], en-Mg_2(dobpdc) [28], and Mg_2(dobdc)$(N_2H_4)_{1.8}$ [35]. Nevertheless, the previously reported amine-decorated MOFs displayed relatively high heat of adsorption (even up to ~120 kJ mol^{-1} [35]) owing to the strong interaction between the amine molecules and CO_2, which requires high energy for adsorbent regeneration process [19,76]. Hence, the development of adsorbents with high CO_2 uptake capacity, CO_2/N_2 selectivity, CO_2 working capacity, and good stability remains a challenge.

In the current work, we effectively prepared a novel hydroxyl (OH)-incorporated MIL-101(Cr)-NH_2 material. Introduction of 2,5-dihydroxylterephthalic acid containing numerous OH functional groups into the MOF generated more CO_2 adsorption sites. Amine-functionalized MIL-101(Cr) displays good moisture-resistivity, which is beneficial for its practical applicability [32,36]. Furthermore, MIL-101(Cr)-NH_2 exhibits a three-dimensional network formed from amine-based linkers that can act as Lewis bases and enhance the CO_2 adsorption ability [51,52]. The prepared $(HO)_2$BDC@CrN adsorbents were employed for CO_2 and N_2 adsorption at different temperatures to evaluate the CO_2 adsorption capability as well as to investigate the separation of CO_2 from a mixture containing N_2 gas. The ideal adsorbed solution theory was utilized to predict the adsorption isotherm of the gas mixture and CO_2/N_2 selectivity. In addition, the isosteric heat of CO_2 adsorption on the parent MIL-101(Cr)-NH_2 and $(HO)_2$BDC@CrN was estimated. Finally, the cycling stability of the synthesized adsorbent was assessed through a series of CO_2 adsorption-desorption cycles.

EXPERIMENTAL

1. Materials

$Cr(NO_3)\cdot 9H_2O$ (99%), 2-aminoterephtalic acid (98%), and 2,5-dihydroxyterephthalic acid ($(HO)_2$BDC, 98%) were purchased from Sigma-Aldrich, USA. *N*,*N*-dimethylmethanamide (DMF, 99.5%) and ethanol (EtOH, 99.5%) were obtained from Daejung Chemical Co., Korea. Ultrahigh-purity CO_2 (99.99%) and N_2 (99.99%) were used for gas adsorption measurements.

2. Synthesis of Amine-functionalized MIL-101(Cr)

Amine-functionalized MIL-101(Cr) (MIL-101(Cr)-NH_2) was synthesized by solvothermal synthesis. Firstly, $Cr(NO_3)_3\cdot 9H_2O$ (5 mmol) and 2-aminoterephthalic acid (ABDC, 5 mmol) were dispersed in deionized water (30 mL) under stirring. The resultant mixture was subsequently sonicated for 10 min, transferred to a Teflon-lined stainless steel autoclave, and maintained at 140 °C for 20 h. The reactor was then gradually cooled to room temperature. The resulting green product was collected and purified using DMF and EtOH at 65 °C for 6 h. Finally, the as-prepared solid was dried at 75 °C in air for 12 h. Prior to analysis, the synthesized samples were degassed at 140 °C for 12 h under vacuum (10^{-2} kPa).

3. Synthesis of $(HO)_2$BDC@CrN-x

$(HO)_2$BDC was incorporated into the MIL-101(Cr)-NH_2 framework during the solvothermal synthesis of MIL-101(Cr)-NH_2. A mixture containing the ABDC ligand (5 mmol) and a desired amount of $(HO)_2$BDC was added to the chromium salt solution prior to the reaction. After the reaction was completed, the green product was collected and washed with DMF and EtOH. The prepared $(HO)_2$DBC-incorporated MIL-101(Cr)-NH_2 adsorbents containing different contents of $(HO)_2$BDC were denoted as $(HO)_2$DBC@CrN-x, where x is the weight percentage of $(HO)_2$BDC loaded during the synthesis (x=4, 8, 12, and 16 wt%).

4. Characterization

X-ray diffraction (XRD) analysis was conducted on MAC-18XHF (Rigaku, Japan) using Cu-K_α radiation. Scanning electron microscopy (SEM) evaluation was performed using a field emission scanning electron microscope (FESEM) (Leo-Supra 55, Carl Zeiss STM, Germany). The N_2 sorption isotherms at 77 K were obtained using Micromeritics instruments (BELSORP-max, BEL, Japan). The surface area was estimated employing the multiple-point Brunauer-Emmett-Teller (BET) method in the pressure range of $0.05<P/P_0<0.20$. Fourier transform-infrared (FT-IR) spectroscopy was carried out on a Tensor 27 spectrophotometer (Bruker, Germany). The chemical states of the elements were analyzed employing X-ray photoelectron spectrometry (XPS) (K-Alpha, Thermo Scientific, USA). Single CO_2 and N_2 adsorption isotherm was measured using an adsorption analyzer (BELSORP-mini II, Bel, Japan). Temperature programmed desorption (TPD) experiments were carried out with helium as a carrier gas and at a heating rate of 4 K min^{-1} using an Auto Chem II 2920 instrument equipped with a thermal conductivity detector (TCD) (Micromeritics, Norcross, GA).

RESULTS AND DISCUSSION

1. Characterization of MIL-101(Cr)-NH_2 and $(HO)_2$BDC@CrN-x

The surface components and chemical states of as-synthesized MIL-101(Cr)-NH_2 were evaluated by XPS (Fig. 1). The survey spectrum revealed that the sample contained Cr, O, C, and N, which is in good agreement with the EDX elemental maps of MIL-101(Cr)-NH_2 (Fig. S1). It is noteworthy that the deconvolution of the C 1s peak resulted in three peaks (Fig. 1(b)). The two peaks at 285.7 and 288.6 eV corresponded to the carbon atoms in the benzene ring and the carboxyl group, respectively. On the other hand, the peak at 284.6 eV was attributed to adventitious carbon [17,55]. Fig. 1(c) illustrates the O 1s spectrum with a single peak at 531.6 eV, which was ascribed to the Cr-O bond [17,64]. As can be seen in Fig. 1(d), the spectrum of Cr 2p displays two peaks at 585.3 eV (Cr $2p_{1/2}$) and 576.6 eV (Cr $2p_{3/2}$), which indicates the presence of Cr(III) [55].

Furthermore, Fig. 2 demonstrates electron micrographs of the prepared amino-functional MIL-101(Cr) and $(HO)_2$BDC@CrN samples. MIL-101(Cr)-NH_2 had aggregated spheroidal particles in the range of 20-100 nm. The $(HO)_2$BDC-incorporated MIL-101(Cr)-NH_2 samples exhibited slightly smaller crystallite sizes with reduced aggregation, indicating that the presence of the $(HO)_2$BDC species influenced the crystallization of MOF. Fig. 3 illustrates the XRD patterns of the synthesized samples. The main diffraction peaks corresponding to amino-functional MIL-101(Cr) are similar to those of the previously reported MIL-101(Cr)-NH_2 frameworks [6,24, 36]. The incorporation of the $(HO)_2$BDC molecules into the amine-functionalized MIL-101(Cr) framework caused a shift of the XRD peaks and marginally decreased peak intensity. A similar phenomenon was also observed for 2,5-dihydroxyterephthalic acid-incor-

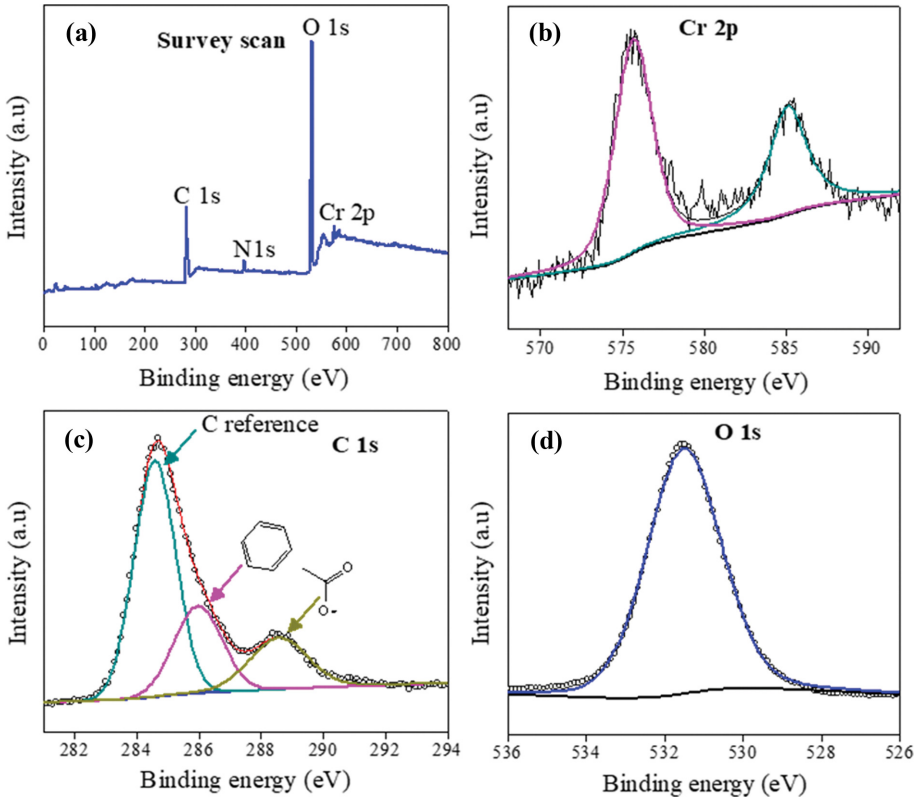

Fig. 1. XPS analysis of the prepared MIL-101(Cr)-NH_2: (a) Survey scan, (b) Cr 2p, (c) C 1s, and (d) O 1s.

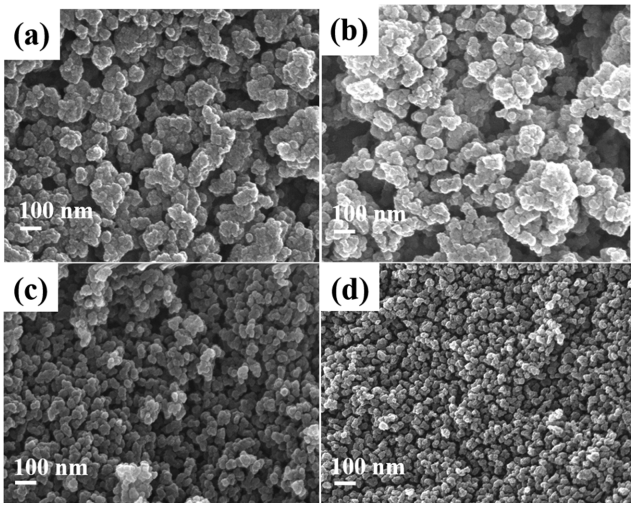

Fig. 2. SEM images of (a) MIL-101(Cr)-NH_2, (b) $(HO)_2$BDC@CrN-4, (c) $(HO)_2$BDC@CrN-12, and (d) $(HO)_2$BDC@CrN-16.

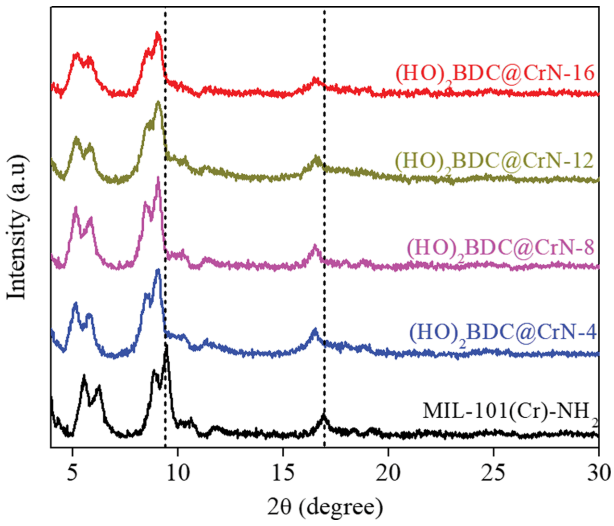

Fig. 3. X-ray diffraction analyses of MIL-101(Cr)-NH_2 and $(HO)_2$ BDC@CrN.

porated MIL-100(Fe) [40].

To investigate the functional groups present in the prepared MIL-101(Cr)-NH_2 and $(HO)_2$BDC@CrN samples, we subsequently conducted FT-IR spectroscopy analysis (Fig. 4). The FT-IR spectrum of the pristine amine-functionalized MIL-101(Cr) displays characteristic peaks for an MIL-101(Cr) framework, with strong bands in the range of 1,600-1,400 cm^{-1} owing to the vibrations of the O-C-O bonds [14,68]. The vibration bands at approximately 3,420 and 3,380 cm^{-1} were ascribed to the asymmetrical and symmetrical stretching vibrations of the amine moieties, respectively (see expansion in Fig. 4) [36,59]. The lower vibrational modes at 1,626 and 1,586 cm^{-1} corresponded to σ(N-H). Moreover, two peaks at 1,337 and 1,256 cm^{-1} were attributed to υ(C-N) of the aromatic amines [23,42,46]. As shown in Fig. 4(A), the spectra of $(HO)_2$ BDC@CrN displayed lower peak intensities compared to those of the pristine MOF, indicating that 2,5-dihydroxylterephtalic acid

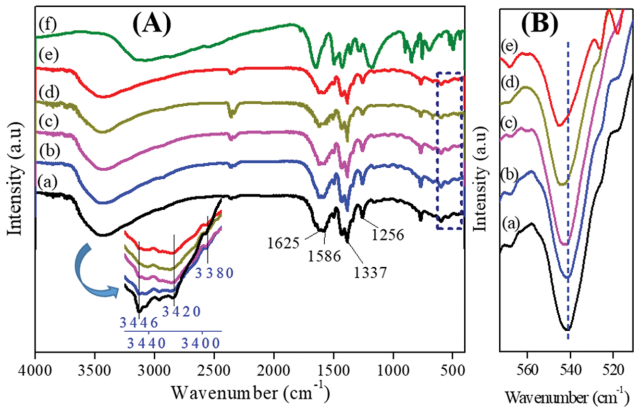

Fig. 4. FT-IR analyses of (a) MIL-101(Cr)-NH_2, (b) $(HO)_2$BDC@CrN-4, (c) $(HO)_2$BDC@CrN-8, (d) $(HO)_2$BDC@CrN-12, (e) $(HO)_2$BDC@CrN-16, and (f) $(HO)_2$BDC.

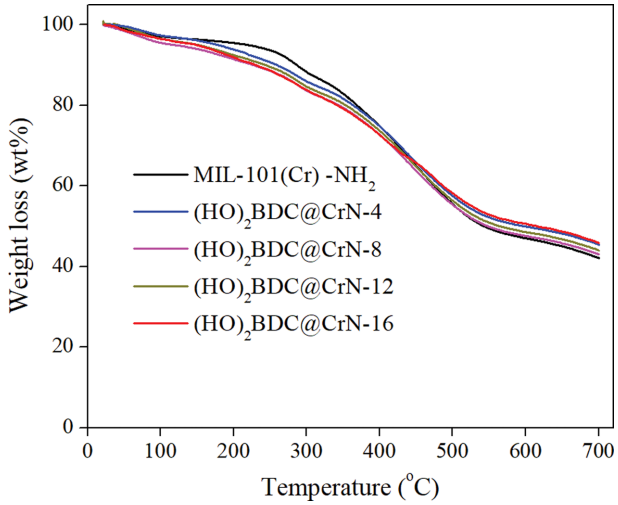

Fig. 5. Thermogravimetric analyses of the synthesized $(HO)_2$BDC@CrN adsorbents.

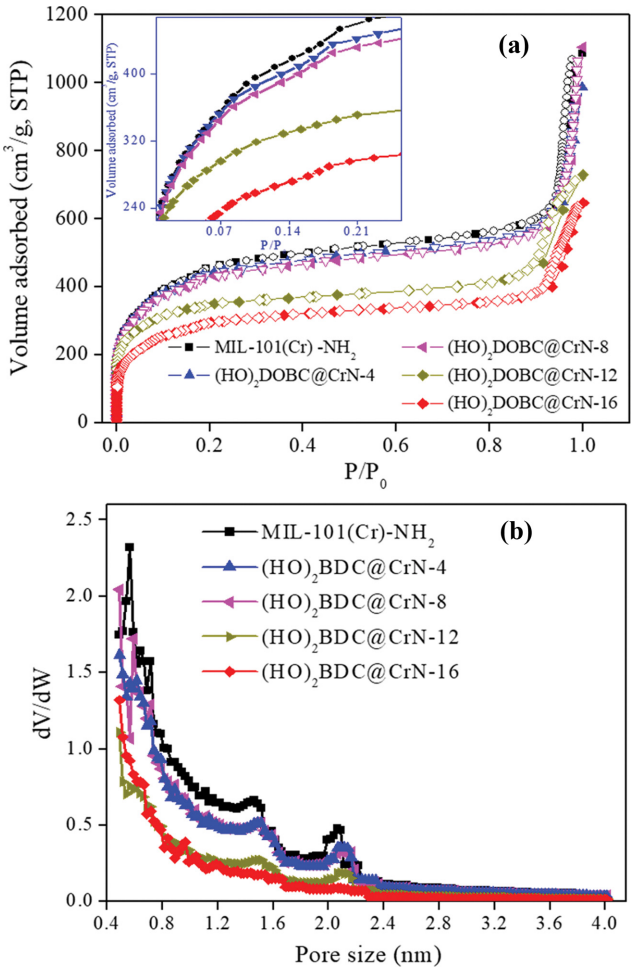

Fig. 6. Textural properties of the MIL-101(Cr)-NH_2 and $(HO)_2$BDC@CrN adsorbents: (a) N_2 adsorption-desorption and (b) pore size distribution.

was incorporated into the MIL-101(Cr)-NH_2 framework. The peak at approximately 540 cm^{-1} was attributed to the Cr-O bond [11,26,56,68] and was marginally shifted toward higher wavenumber with increasing $(HO)_2$BDC content (Fig. 4(B)). The reason for the shift could be the interaction between the $(HO)_2$BDC molecules and the Cr^{3+} metal ions. In addition, the peaks corresponding to the Cr-O bonds included the possible Cr-O bonds between Cr and the ABDC ligand as well as the Cr-O bonds between Cr and the $(HO)_2$BDC molecule.

Fig. 5 demonstrates the TGA profiles of the $(HO)_2$BDC@CrN samples and MIL-101(Cr)-NH_2. As can be seen, the TGA curve of MIL-101(Cr)-NH_2 exhibits three weight loss steps. The first weight loss between 25 and 110 °C was attributed to the release of solvent molecules, including water and ethanol. The next weight loss observed from 110 to 275 °C was a consequence of the dehydroxylation of the chromium oxo-clusters. Notably, the most significant weight loss step started at approximately 280 °C and corresponded to the decomposition of the organic linkers in the framework [36]. The thermal stability of the $(HO)_2$BDC@CrN samples was similar to that of MIL-101(Cr)-NH_2. However, unlike the case of pure MIL-101(Cr)-NH_2, the last stage on the TGA curve of $(HO)_2$BDC@CrN was not preceded by a clear plateau, suggesting that the frameworks started to decompose before the solvent was completely removed. This could be due to the strong interaction between the solvents and the $(HO)_2$DBC molecules incorporated into the MOF.

Fig. 6(a) and (b) illustrate the N_2 isotherms and pore size distribution of the synthesized MIL-101(Cr)-NH_2 and $(HO)_2$BDC@CrN materials. All isotherms exhibited a typical type I with an H3-type hysteresis loop, indicating the presence of slit-like pores within the MIL-101(Cr) framework [61,67]. The isotherm displays a sharp uptake at very low P/P_0 values, which is a feature characteristic of microporous supertetrahedra [36]. Additionally, the secondary uptake at P/P_0=0.1 and P/P_0=0.2 (the inset of Fig. 6(a)) was assigned to the presence of two kinds of nanoporous windows in the framework. This is consistent with the previous reports on the structures of MIL-101(Cr) [7,55] and amine-functionalized MIL-101(Cr) [6,36]. As demonstrated in Fig. 6(a), the amount of adsorbed N_2 in $(HO)_2$BDC-incorporated MIL-101(Cr)-NH_2 decreased with increasing $(HO)_2$BDC concentration. Table 1 summarizes the BET surface area and total pore volume of the analyzed

Table 1. Textural properties of the MIL-101(Cr)-NH_2 and $(HO)_2$BDC@CrN adsorbents

Sample	S_{BET}, $m^2\ g^{-1}$	Total pore volume, $cm^3\ g^{-1}$
MIL-101(Cr)-NH_2	1,725	1.55
$(HO)_2$BDC@CrN-4	1,610	1.40
$(HO)_2$BDC@CrN-8	1,560	1.37
$(HO)_2$BDC@CrN-12	1,120	1.08
$(HO)_2$BDC@CrN-16	985	0.82

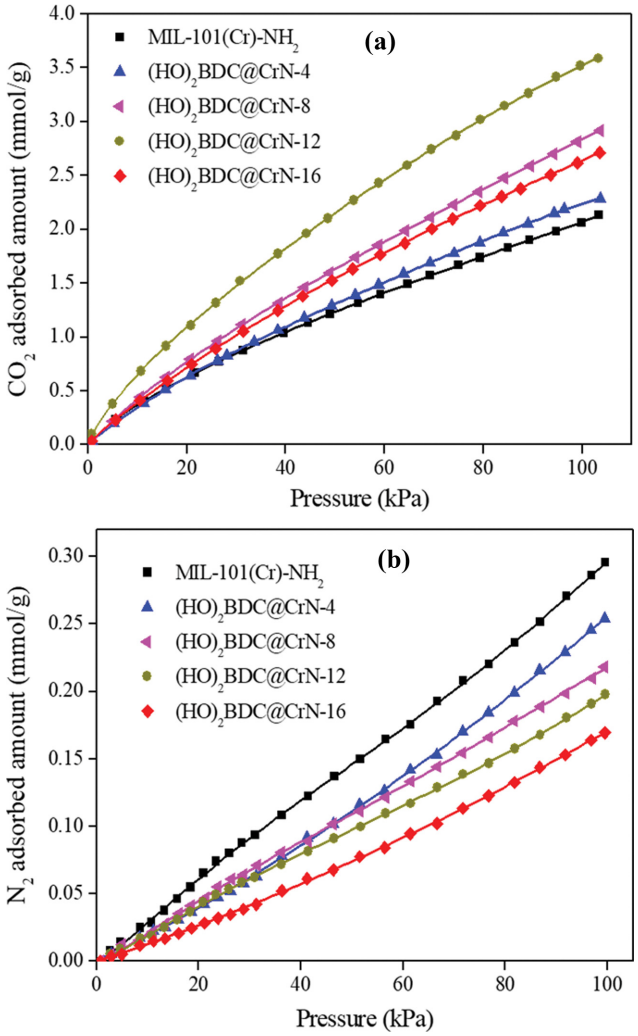

Fig. 7. CO_2 and N_2 adsorption isotherms of MIL-101(Cr)-NH_2 and $(HO)_2$BDC@CrN at 298 K on: (a) CO_2 and (b) N_2. The solid lines were fitted from the DSLF model.

samples. The parent amine-functionalized MIL-101(Cr) exhibited a BET surface area and pore volume of 1,725 $m^2\ g^{-1}$ and 1.55 $cm^3\ g^{-1}$, respectively, which were comparable to those previously reported for MIL-101(Cr)-NH_2 [36]. The BET surface area and pore volume of the $(HO)_2$BDC@CrN samples decreased with increasing amount of $(HO)_2$BDC. In particular, increasing the content of $(HO)_2$BDC from 4 wt% to 8, 12, and 16 wt% resulted in a decrease in the BET surface area from 1,610 $m^2\ g^{-1}$ to 1,560, 1,120, and 985 $m^2\ g^{-1}$, respectively. Moreover, the pore volume decreased

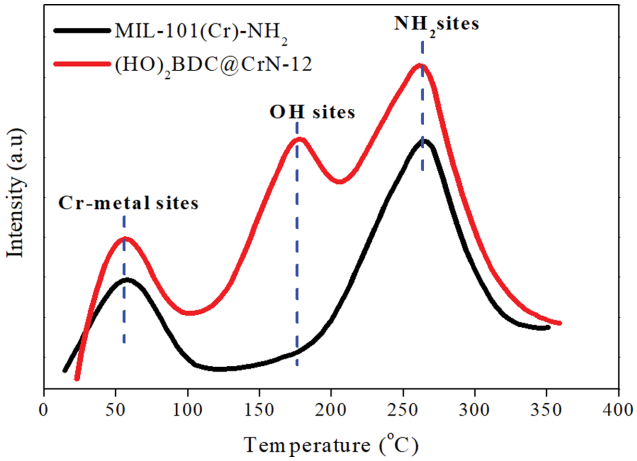

Fig. 8. CO_2-TPD profiles of CO_2 adsorbed on MIL-101(Cr)-NH_2 and $(HO)_2$BDC@CrN.

from 1.40 $cm^3\ g^{-1}$ to 1.37, 1.08, and 0.82 $cm^3\ g^{-1}$, respectively.

2. CO_2 and N_2 Adsorption

Fig. 7(a) and (b) illustrate the adsorption isotherms of gaseous CO_2 and N_2 at 298 K. At 100 kPa, pristine MIL-101(Cr)-NH_2 displayed CO_2 adsorption capacity of 2.14 mmol g^{-1}. Notably, the incorporation of the $(HO)_2$BDC molecules into the framework of MIL-101(Cr)-NH_2 increased the CO_2 adsorption ability of the prepared adsorbent. At 100 kPa, the CO_2 uptake amounts of $(HO)_2$BDC@CrN-4, $(HO)_2$BDC@CrN-8, $(HO)_2$BDC@CrN-12, and $(HO)_2$BDC@CrN-16 were determined at 2.29, 2.71, 3.58, and 2.90 mmol g^{-1}, respectively. The highest CO_2 adsorption capacity of 3.58 mmol g^{-1} was achieved over the $(HO)_2$BDC@CrN-12 adsorbent. In this case, the adsorption capacity was 40% higher than that of the MIL-101(Cr)-NH_2 sample, also surpassing those of other reported adsorbents, including activated carbon, nitrogen-doped hollow carbon, zeolite, ZIF-68, MOF-5, ZIF-8, UiO-66(Zr), and MIL-100(Cr) (Table 2). It is noteworthy that the $(HO)_2$BDC-containing adsorbents exhibited lower BET surface areas and pore volumes than the parent MIL-101(Cr)-NH_2. It was found that the adsorption ability of the adsorbents toward CO_2 was predominantly dependent on its porosity and surface chemistry [40,66]. As mentioned, the incorporation of the $(HO)_2$BDC molecules into MIL-101(Cr)-NH_2 not only decreased the surface area and pore volume, but also altered the surface chemistry due to the presence of numerous hydroxyl and carboxylic functional groups in the $(HO)_2$BDC molecules. Hence, the increase of the CO_2 adsorption ability of the resulting $(HO)_2$BDC@CrN samples could be attributed to the generation of more adsorptive sites on the $(HO)_2$BDC@CrN adsorbents. To validate this hypothesis, CO_2- temperature programmed-desorption (TPD) experiments were conducted on the MIL-101(Cr)-NH_2 and $(HO)_2$BDC@CrN-12 samples (Fig. 8). The CO_2-TPD curve of MIL-101(Cr)-NH_2 displayed two desorption peaks at 56 °C and 268 °C, which were assigned to desorption of CO_2 adsorbed on the unsaturated Cr-metal and amine sites, respectively [70,76]. On the other hand, the CO_2-TPD curve of $(HO)_2$BDC@CrN exhibited a new CO_2 desorption peak at approximately 165 °C, which corresponded to the presence of hydroxyl sites. A similar phenomenon was reported for the 2,5-dihydroxytereph-

Table 2. CO_2 adsorption capacity on different adsorbents for comparison

Adsorbent	CO_2 adsorption capacity (mmol g^{-1}) at 100 kPa	Temperature, K	Refs.
MCM-41	0.67	298	[72]
Activated carbon	2.0	298	[49]
SiO_2-NS	4.0	348	[47]
ZSM	1.6	303	[33]
ZIF-68	1.7	298	[4]
MOF-5	2.10	296	[69]
UiO-66(Zr)	2.16	298	[34]
UiO-66(Zr)-NH_2	2.8	298	[21]
UiO-66(Zr)/GO	3.37	298	[9]
Nitrogen-doped hollow carbon	2.67	298	[15]
MIL-100(Cr)	1.6	308	[8]
EN-MIL-100(Cr)	2.4	308	[8]
MIL-101(Cr)	3.24	298	[75]
ZIF-8	0.15	298	[39]
67MIL-101(Cr)@Fs	2.13	298	[75]
MIL-101(Cr,Mg)	3.28	298	[76]
DOBDC@MIL-100(Fe)	3.63	298	[40]
MIL-101(Cr)-NH_2	2.14	298	This work
$(HO)_2$BDC@CrN-12	3.58	298	This work

thalic acid-incorporated MIL-100(Fe) adsorbent [40]. The CO_2 desorption temperature determined based on the CO_2-TPD profiles revealed that the interaction between CO_2 and the incorporated hydroxyl sites of $(HO)_2$BDC@CrN was stronger than that between the gas and the unsaturated Cr-metal sites; however, it was weaker than the interaction with the amine sites. Based on the assumption that all the $(HO)_2$(BDC) ligands were successfully incorporated into MIL-101(Cr)-NH_2 framework, the concentration of OH site was derived from the loading amount of $(HO)_2$BDC to further evaluate its influence on the adsorbent's performance (Fig. 9). From Fig. 9, it can be observed that the CO_2 adsorption capacity at 100 kPa increased with an increase OH site concentration

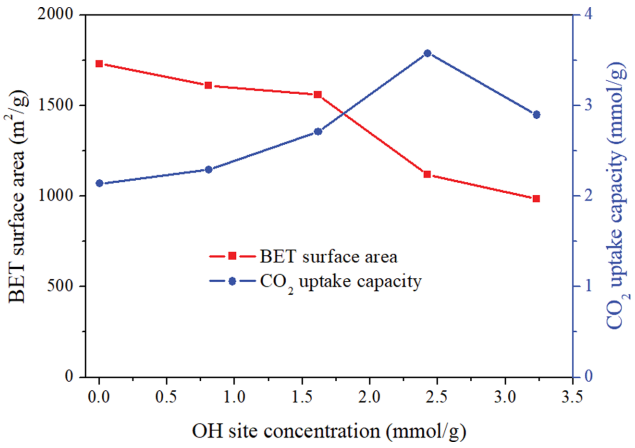

Fig. 9. Surface area and CO_2 adsorption capacity at 100 kPa of $(HO)_2$BDC@CrN adsorbents as a function of the OH site concentration.

from 0 to 2.4 mmol g^{-1} although the BET surface area of the adsorbent decreased. Further increasing the OH site concentration up to 3.2 mmol g^{-1} (16 wt% of $(HO)_2$BDC)), the CO_2 uptake capacity began to decrease due to the pore blockage and/or thickened diffusion path length [55,66]. In contrast to CO_2, increasing the $(HO)_2$BDC loading amount led to a considerable decrease in the N_2 adsorption capacity. The possible explanation for this observation was the significant role of porosity in nitrogen adsorption, the driving forces of which are weak van der Waals interactions [37, 44,76].

To express the adsorption behavior of pure CO_2 and N_2, the isotherm data were fitted with various models such as the Langmuir, Freundlich, or Dual-site Langmuir Freundlich (DSLF) models. Among them, the DSLF model was found to be the best for describing CO_2 and N_2 adsorption on MIL-101(Cr)-NH_2 and $(HO)_2$BDC@CrN. The DSLF equation can be expressed as follows [43, 44,50]:

$$q = q_{s,1}\frac{k_1 p^{1/n_1}}{1+k_1 p^{1/n_1}} + q_{s,2}\frac{k_2 p^{1/n_2}}{1+k_2 p^{1/n_2}} \quad (1)$$

where q is the adsorption capacity [mmol g^{-1}]; $q_{s,1}$ and $q_{s,2}$ are the saturation capacities of sites 1 and 2, respectively; p is the pressure of bulk gas at equilibrium with the adsorbed phase [kPa]; k_1 and k_2 are the affinity coefficients of sites 1 and 2, respectively [kPa^{-1}]; and n_1 and n_2 are the corresponding deviations from an ideal homogeneous surface. Table S1 lists the corresponding DSLF fitting parameters for gas adsorption on $(HO)_2$BDC@CrN and MIL-101(Cr)-NH_2 at 298 K. Accordingly, the obtained correlation coefficients (R^2) were very close to 1.0, implying that the CO_2 and N_2 adsorption behavior on both $(HO)_2$BDC@CrN and MIL-101(Cr)-NH_2 can be well described by the dual-site model. The parameters of

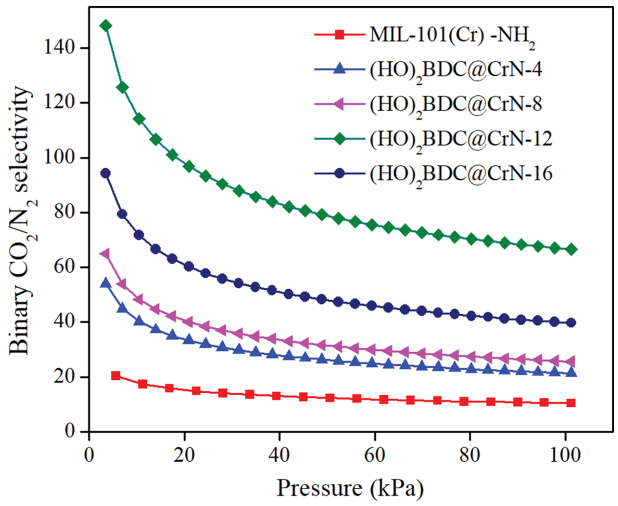

Fig. 10. IAST-predicted CO_2/N_2 selectivity of the CO_2/N_2 mixture (0.15/0.85) on the MIL-101(Cr)-NH_2 and $(HO)_2$BDC@CrN adsorbents.

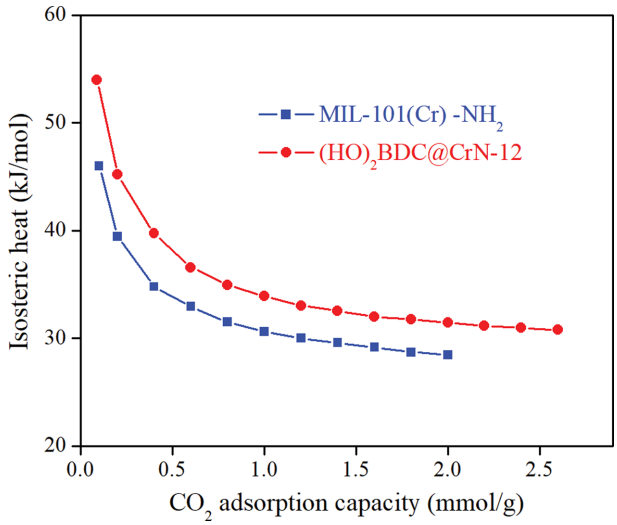

Fig. 12. Isosteric heat of CO_2 adsorption on MIL-101(Cr)-NH_2 and $(HO)_2$BDC@CrN-12.

DSLF equation described gas adsorption on $(HO)_2$BDC@CrN were different from those recorded on MIL-101(Cr)-NH_2. For instance, the saturation capacity for CO_2 on $(HO)_2$BDC@CrN was higher than that for CO_2 on MIL-101(Cr)-NH_2, indicating that the CO_2 adsorption on the surface of $(HO)_2$BDC@CrN was enhanced compared to that of parent MIL-101(Cr)-NH_2. The obtained fitting parameters were then combined with IAST to predict the adsorption isotherms and ultimately calculate the IAST selectivities ($[(n_{CO_2}/n_{N_2})/(p_{CO_2}/p_{N_2})]$) for the CO_2/N_2 mixture (0.15/0.85) at 298 K on the parent MIL-101(Cr)-NH_2 and $(HO)_2$BDC@CrN samples (Fig. 10). As demonstrated in Fig. 10, the CO_2/N_2 selectivity of the $(HO)_2$BDC-containing adsorbents was considerably higher than that of the sole MIL-101(Cr)-NH_2 in the entire pressure range. At 100 kPa, the highest CO_2/N_2 adsorption selectivity of ~67 was achieved for $(HO)_2$BDC@CrN-12, which was six times higher than the adsorption selectivity of MIL-101(Cr)-NH_2.

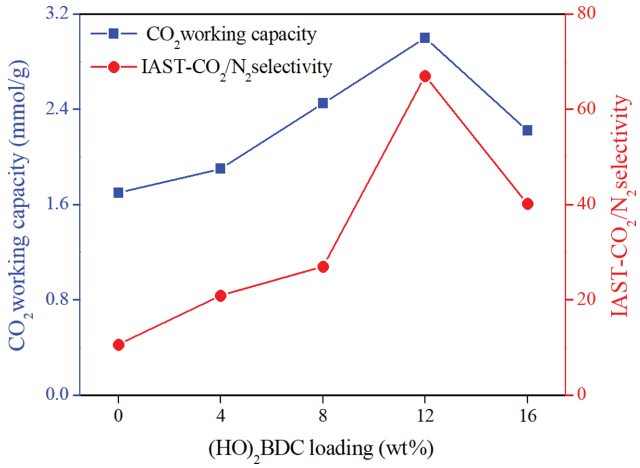

Fig. 11. Effects of $(HO)_2$BDC loading on the working capacity of CO_2 and the CO_2/N_2 selectivity.

In addition to gas selectivity, the CO_2 adsorption working capacity is a practically important parameter for evaluating adsorbents [55,65]. Based on the pure CO_2 adsorption isotherm, CO_2 working capacity for MIL-101(Cr)-NH_2 and $(HO)_2$BDC@CrN-x adsorbents was estimated between 100 and 10 kPa. Fig. 11 demonstrates the IAST-predicted CO_2/N_2 selectivity and CO_2 adsorption working capacity of the investigated adsorbents. Both the CO_2/N_2 selectivity and CO_2 working capacity increased when the $(HO)_2$BDC loading increased up to 12 wt%. However, at higher $(HO)_2$BDC loading, the CO_2 working capacity decreased. Considering the CO_2 adsorption capacity, working capacity, and CO_2/N_2 selectivity, the resultant $(HO)_2$BDC@CrN-12 material was the best adsorbent among the investigated samples.

The CO_2 adsorption isotherms of the parent MIL-101(Cr)-NH_2 and $(HO)_2$BDC@CrN-12 (Fig. S2) at different temperatures were used to estimate the isosteric heat of adsorption of CO_2 on the analyzed materials utilizing the Clausius-Clapeyron equation [40,44] (Fig. 12). The isosteric heat of CO_2 adsorption on $(HO)_2$BDC@CrN-12 was higher than that on the pristine MOF, indicating that $(HO)_2$BDC@CrN interacted with CO_2 more strongly than MIL-101(Cr)-NH_2. Moreover, at low coverage, the heat of CO_2 adsorption on MIL-101(Cr)-NH_2 was 46 kJ mol^{-1}, which was consistent with the heat of CO_2 adsorption reported for MIL-101(Cr)-NH_2 [36] and several other amine-functionalized MOFs [51]. The synthesized $(HO)_2$BDC@CrN-12 exhibited heat of CO_2 adsorption of 54 kJ mol^{-1}, which was higher than that of MIL-101(Cr)-NH_2. This was attributed to the addition of more polar functional groups into the MIL-101(Cr)-NH_2 framework, which resulted in enhanced interaction between the adsorbent and the CO_2 molecules [18]. As evidenced by the CO_2-TPD measurements, the presence of the hydroxyl sites on $(HO)_2$BDC@CrN-12 induced stronger interaction with CO_2 than with the Cr-metal sites; however, the interactions were weaker than with the amine sites. Furthermore, the heat of CO_2 adsorption of $(HO)_2$BDC@CrN-12 was higher than that of MIL-101(Cr) (33 kJ mol^{-1}), MIL-101(Cr, Mg) (35 kJ mol^{-1}) [76], DOBDC@MIL-100(Fe) (33 kJ mol^{-1}) [40], and GrO@MIL-

101(Cr) (45 kJ mol^{-1}) [74]. Conversely, the heat of CO_2 adsorption of the material was lower than that of some amine-decorated MOFs, such as mmen-Mg_2(dobpdc) (71 kJ mol^{-1}) [20] or Mg_2(dobdc)$(N_2H_4)_{1.8}$ (120 kJ mol^{-1}) [35].

3. Regeneration of the Adsorbent

Several CO_2 adsorption-desorption cycles were performed to elucidate the regenerability of the prepared $(HO)_2$BDC@CrN-12 adsorbent. After each adsorption-desorption measurement at 298 K, the adsorbent was further heated at 100 °C for 60 min under vacuum (10^{-2} kPa) to ensure that the adsorbed CO_2 was recovered. The regenerated adsorbent was subsequently used for another CO_2 adsorption-desorption measurement. As demonstrated in Fig. 13(a), small hysteresis was observed between the adsorption and desorption curves, and the adsorbed amount of CO_2 in the low-pressure regime was slightly decreased after the first cycle. This could be due to the strong interaction between amine group in MIL-101(Cr)-NH_2 framework and CO_2, which caused incomplete desorption of the adsorbed CO_2 molecules at the mild condition of 298 K [19, 76]. After six consecutive adsorption-desorption cycles, the total CO_2 capture capacity of $(HO)_2$BDC@CrN-12 was estimated at approximately 96% of the maximum adsorbed amount (Fig. 13(b)). This result suggests that the CO_2 capacity loss after six adsorption-desorption cycles was negligible.

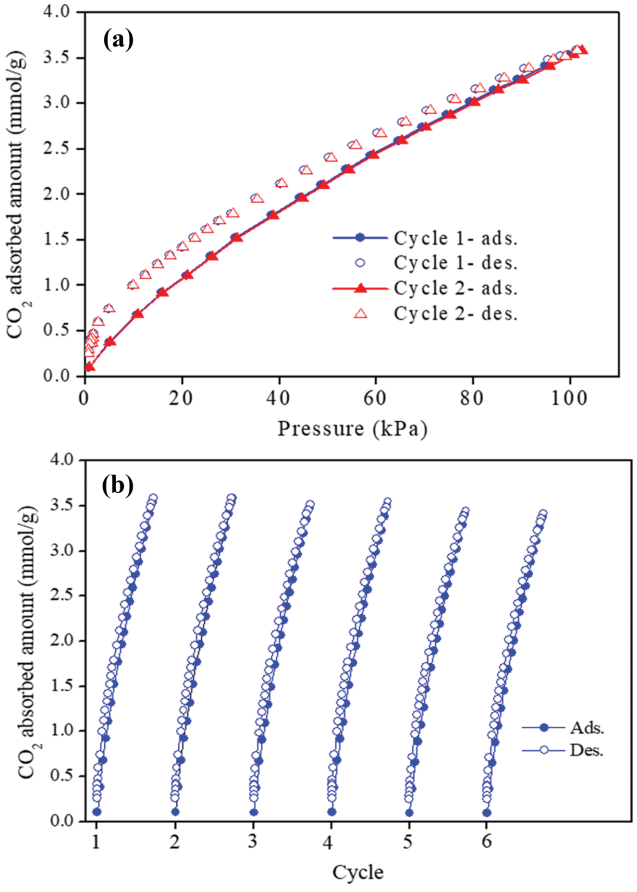

Fig. 13. CO_2 adsorption-desorption: (a) The first and second adsorption-desorption curves, and (b) six adsorption-desorption cycles.

CONCLUSIONS

A 2,5-dihydroxylterephthalic acid-incorporated MIL-101(Cr)-NH_2 framework was successfully prepared via a one-pot synthesis. Increasing the loading amount of $(HO)_2$BDC on MIL-101(Cr)-NH_2 from 4 to 16 wt% resulted in a decrease of the surface area and pore volume from 1,610 to 985 m^2 g^{-1} and from 1.40 to 0.82 cm^3 g^{-1}, respectively. The CO_2 adsorption capacity was considerably improved on $(HO)_2$BDC@CrN due to the incorporation of hydroxyl sites inside the framework. The optimum adsorbent, i.e., $(HO)_2$BDC@CrN-12 containing 2.4 mmol g^{-1} of OH site, exhibited 40% higher CO_2 uptake capacity and six times higher CO_2/N_2 selectivity than that of MIL-101(Cr)-NH_2. Notably, the synthesized $(HO)_2$BDC@CrN adsorbent displayed good regenerability after six adsorption-desorption cycles. The obtained results suggest that the surface modification of MOFs with hydroxyl group-containing guest molecules is a promising strategy for the preparation of CO_2-selective adsorption materials.

ACKNOWLEDGEMENT

This work was supported by the Industrial University of Ho Chi Minh City, Vietnam (19.2H02).

SUPPORTING INFORMATION

Additional information as noted in the text. This information is available via the Internet at http://www.springer.com/chemistry/journal/11814.

REFERENCES

1. S. Bae, N. Zaini, K. S. N. Kamarudin, K. S. Yoo, J. Kim and M. R. Othman, *Korean J. Chem. Eng.*, **35**, 764 (2018).
2. Y.-S. Bae, B. G. Hauser, O. K. Farha, J. T. Hupp and R. Q. Snurr, *Micropor. Mesopor. Mater.*, **141**, 231 (2011).
3. Y.-S. Bae and R. Q. Snurr, *Angew. Chem. Int. Ed.*, **50**, 11586 (2011).
4. R. Banerjee, H. Furukawa, D. Britt, C. Knobler, M. O'Keeffe and O. M. Yaghi, *J. Am. Chem. Soc.*, **131**, 3875 (2009).
5. Z. Bao, L. Yu, Q. Ren, X. Lu and S. Deng, *J. Colloid Interface Sci.*, **353**, 549 (2011).
6. S. Bernt, V. Guillerm, C. Serre and N. Stock, *Chem. Commun.*, **47**, 2838 (2011).
7. S. Bhattacharjee, C. Chen and W.-S. Ahn, *RSC Adv.*, **4**, 52500 (2014).
8. C. P. Cabello, G. Berlier, G. Magnacca, P. Rumori and G. T. Palomino, *CrystEngComm.*, **17**, 430 (2015).
9. Y. Cao, Y. Zhao, Z. Lv, F. Song and Q. Zhong, *J. Ind. Eng. Chem.*, **27**, 102 (2015).
10. Y. Cao, Y. Zhao, F. Song and Q. Zhong, *J. Energy Chem.*, **23**, 468 (2014).
11. Y. Chen, K. Ding, L. Yang, B. Xie, F. Song, J. Wan, G. Wang and M. Han, *Appl. Phys. Lett.*, **92**, 173112 (2008).
12. V. Chernikova, O. Yassine, O. Shekhah, M. Eddaoudi and K. N. Salama, *J. Mater. Chem. A*, **6**, 5550 (2018).
13. J. B. DeCoste, G. W. Peterson, B. J. Schindler, K. L. Killops, M. A. Browe and J. J. Mahle, *J. Mater. Chem. A*, **1**, 11922 (2013).

14. A. T. Ezhil Vilian, B. Dinesh, R. Muruganantham, S. R. Choe, S.-M. Kang, Y. S. Huh and Y.-K. Han, *Microchim. Acta*, **184**, 4793 (2017).
15. S. Feng, W. Li, Q. Shi, Y. Li, J. Chen, Y. Ling, A. M. Asiri and D. Zhao, *Chem. Commun.*, **50**, 329 (2014).
16. H. Furukawa, K. E. Cordova, M. O'Keeffe and O. M. Yaghi, *Science*, **341**, 1230444 (2013).
17. H. Guo, D. Wang, J. Chen, W. Weng, M. Huang and Z. Zheng, *Chem. Eng. J.*, **289**, 479 (2016).
18. Z. Hu, Y. Peng, Z. Kang, Y. Qian and D. Zhao, *Inorg. Chem.*, **54**, 4862 (2015).
19. Z. Hu, Y. Wang, S. Farooq and D. Zhao, *AIChE J.*, **63**, 4103 (2017).
20. Z. Hu, Y. Wang, B. B. Shah and D. Zhao, *Adv. Sustain. Syst.*, **3**, 1800080 (2019).
21. A. Huang, L. Wan and J. Caro, *Mater. Res. Bull.*, **98**, 308 (2018).
22. W. Huang, X. Zhou, Q. Xia, J. Peng, H. Wang and Z. Li, *Ind. Eng. Chem. Res.*, **53**, 11176 (2014).
23. N. Janakiraman and M. Johnson, *Rom. J. Biophys.*, **25**, 131 (2015).
24. D. Jiang, L. L. Keenan, A. D. Burrows and K. J. Edler, *Chem. Commun.*, **48**, 12053 (2012).
25. Y. Jiao, C. R. Morelock, N. C. Burtch, W. P. Mounfield, J. T. Hungerford and K. S. Walton, *Ind. Eng. Chem. Res.*, **54**, 12408 (2015).
26. H. Kumar, P. N. Tengli, V. K. Mishra, P. Tripathi, D. B. Pal and P. K. Mishra, *RSC Adv.*, **7**, 12486 (2017).
27. V. N. Le, H. T. Kwon, T. K. Vo, J.-H. Kim, W.-S. Kim and J. Kim, *Mater. Chem. Phys.*, **253**, 123278 (2020).
28. W. R. Lee, S. Y. Hwang, D. W. Ryu, K. S. Lim, S. S. Han, D. Moon, J. Choi and C. S. Hong, *Energy Environ. Sci.*, **7**, 744 (2014).
29. J. Lei, S. Wang and J. Li, *Chem. Eng. Sci.*, **220**, 115654 (2020).
30. H. Li, K. Wang, Y. Sun, C. T. Lollar, J. Li and H.-C. Zhou, *Mater. Today*, **21**, 108 (2018).
31. J.-R. Li, J. Sculley and H.-C. Zhou, *Chem. Rev.*, **112**, 869 (2012).
32. N. Li, J. Xu, R. Feng, T.-L. Hu and X.-H. Bu, *Chem. Commun.*, **52**, 8501 (2016).
33. Y. Li, H. Yi, X. Tang, F. Li and Q. Yuan, *Chem. Eng. J.*, **229**, 50 (2013).
34. W. Liang, C. J. Coghlan, F. Ragon, M. Rubio-Martinez, D. M. D'Alessandro and R. Babarao, *Dalton Trans.*, **45**, 4496 (2016).
35. P.-Q. Liao, X.-W. Chen, S.-Y. Liu, X.-Y. Li, Y.-T. Xu, M. Tang, Z. Rui, H. Ji, J.-P. Zhang and X.-M. Chen, *Chem. Sci.*, **7**, 6528 (2016).
36. Y. Lin, C. Kong and L. Chen, *RSC Adv.*, **2**, 6417 (2012).
37. Y. Lin, H. Lin, H. Wang, Y. Suo, B. Li, C. Kong and L. Chen, *J. Mater. Chem. A.*, **2**, 14658 (2014).
38. J. Liu, P. K. Thallapally, B. P. McGrail, D. R. Brown and J. Liu, *Chem. Soc. Rev.*, **41**, 2308 (2012).
39. J. McEwen, J.-D. Hayman and A. O. Yazaydin, *Chem. Phys.*, **412**, 72 (2013).
40. L. Mei, T. Jiang, X. Zhou, Y. Li, H. Wang and Z. Li, *Chem. Eng. J.*, **321**, 600 (2017).
41. I. Mihad, S. Rana and A. H. Ghaleb, *Curr. Med. Chem.*, **24**, 193 (2017).
42. A. Modrow, D. Zargarani, R. Herges and N. Stock, *Dalton Trans.*, **41**, 8690 (2012).
43. V. N. Le, T. K. Vo, J. H. Lee, J. C. Kim, T.-H. Kim, K.-H. Oh, Y.-S. Bae, S.-K. Kwak and J. Kim, *Chem. Eng. J.*, **404**, 126492 (2020).
44. J. Peng, S. Xian, J. Xiao, Y. Huang, Q. Xia, H. Wang and Z. Li, *Chem. Eng. J.*, **270**, 282 (2015).
45. Y.-K. Seo, J. W. Yoon, J. S. Lee, U. H. Lee, Y. K. Hwang, C.-H. Jun, P. Horcajada, C. Serre and J.-S. Chang, *Micropor. Mesopor. Mater.*, **157**, 137 (2012).
46. L. Shen, S. Liang, W. Wu, R. Liang and L. Wu, *Dalton Trans.*, **42**, 13649 (2013).
47. Z. Shen, Q. Cai, C. Yin, Q. Xia, J. Cheng, X. Li and Y. Wang, *Chem. Eng. Sci.*, **217**, 115528 (2020).
48. J. M. Simmons, H. Wu, W. Zhou and T. Yildirim, *Energy Environ. Sci.*, **4**, 2177 (2011).
49. R.-L. Tseng, F.-C. Wu and R.-S. Juang, *Sep. Purif. Technol.*, **140**, 53 (2015).
50. N. T. Tran, T. K. Vo, J. Kim and M. R. Othman, *Colloids Surf. A: Physicochem. Eng. Aspects.*, **615**, 126242 (2021).
51. R. Vaidhyanathan, S. S. Iremonger, K. W. Dawson and G. K. H. Shimizu, *Chem. Commun.*, **35**, 5230 (2009).
52. R. Vaidhyanathan, S. S. Iremonger, G. K. H. Shimizu, P. G. Boyd, S. Alavi and T. K. Woo, *Science*, **330**, 650 (2010).
53. T. K. Vo, Y.-S. Bae, B.-J. Chang, S.-Y. Moon, J.-H. Kim and J. Kim, *Micropor. Mesopor. Mater.*, **274**, 17 (2019).
54. T. K. Vo, D. C. Hau, V. C. Nguyen, D. T. Quang and J. Kim, *Appl. Surf. Sci.*, **546**, 149087 (2021).
55. T. K. Vo, J.-H. Kim, H. T. Kwon and J. Kim, *J. Ind. Eng. Chem.*, **80**, 345 (2019).
56. T. K. Vo and J. Kim, *Korean J. Chem. Eng.*, **37**, 571 (2020).
57. T. K. Vo, W.-S. Kim and J. Kim, *Korean J. Chem. Eng.*, **37**, 1206 (2020).
58. T. K. Vo, V. N. Le, V. C. Nguyen, M. Song, D. Kim, K. S. Yoo, B. J. Park and J. Kim, *J. Ind. Eng. Chem.*, **86**, 178 (2020).
59. T. K. Vo, V. N. Le, V. C. Nguyen, M. Song, D. Kim, K. S. Yoo, B. J. Park and J. Kim, *J. Ind. Eng. Chem.*, **86**, 178 (2020).
60. T. K. Vo, V. N. Le, D. T. Quang, M. Song, D. Kim and J. Kim, *Micropor. Mesopor. Mater.*, **306**, 110405 (2020).
61. T. K. Vo, V. N. Le, K. S. Yoo, M. Song, D. Kim and J. Kim, *Cryst. Growth Des.*, **19**, 4949 (2019).
62. T. K. Vo, V. C. Nguyen, D. T. Quang, B. J. Park and J. Kim, *Micropor. Mesopor. Mater.*, **312**, 110746 (2021).
63. T. K. Vo, T. P. Trinh, V. C. Nguyen and J. Kim, *J. Ind. Eng. Chem.*, **95**, 224 (2020).
64. D. Wang, Y. Ke, D. Guo, H. Guo, J. Chen and W. Weng, *Sens. Actuator B-Chem.*, **216**, 504 (2015).
65. S. Xian, Y. Wu, J. Wu, X. Wang and J. Xiao, *Ind. Eng. Chem. Res.*, **54**, 11151 (2015).
66. Q. Yan, Y. Lin, C. Kong and L. Chen, *Chem. Commun.*, **49**, 6873 (2013).
67. J. Yu, S. Wang, J. Low and W. Xiao, *Phys. Chem. Chem. Phys.*, **15**, 16883 (2013).
68. Z. Zhang, X. Li, B. Liu, Q. Zhao and G. Chen, *RSC Adv.*, **6**, 4289 (2016).
69. Z. Zhao, Z. Li and Y. S. Lin, *Ind. Eng. Chem. Res.*, **48**, 10015 (2009).
70. X.-X. Zheng, L.-J. Shen, X.-P. Chen, X.-H. Zheng, C.-T. Au and L.-L. Jiang, *Inorg. Chem.*, **57**, 10081 (2018).
71. R. Zhong, X. Yu, W. Meng, J. Liu, C. Zhi and R. Zou, *ACS Sustain. Chem. Eng.*, **6**, 16493 (2018).
72. J. Zhou, H. Zhao, J. Li, Y. Zhu, J. Hu, H. Liu and Y. Hu, *Solid State Sci.*, **24**, 107 (2013).
73. X. Zhou, W. Huang, J. Liu, H. Wang and Z. Li, *Chem. Eng. Sci.*,

167, 98 (2017).
74. X. Zhou, W. Huang, J. Miao, Q. Xia, Z. Zhang, H. Wang and Z. Li, *Chem. Eng. J.*, **266**, 339 (2015).
75. Z. Zhou, B. Cheng, C. Ma, F. Xu, J. Xiao, Q. Xia and Z. Li, *RSC Adv.*, **5**, 94276 (2015).
76. Z. Zhou, L. Mei, C. Ma, F. Xu, J. Xiao, Q. Xia and Z. Li, *Chem. Eng. Sci.*, **147**, 109 (2016).
77. R. Zou, A. I. Abdel-Fattah, H. Xu, Y. Zhao and D. D. Hickmott, *CrystEngComm.*, **12**, 1337 (2010).

Supporting Information

Construction of OH sites within MIL-101(Cr)-NH_2 framework for enhanced CO_2 adsorption and CO_2/N_2 selectivity

The Ky Vo*,†, Pham Van Vu*, Van Cuong Nguyen*, and Jinsoo Kim,†**

*Department of Chemical Engineering, Industrial University of Ho Chi Minh City, 12 Nguyen Van Bao, Go Vap, Ho Chi Minh City, Vietnam
**Department of Chemical Engineering (Integrated Engineering), Kyung Hee University, 1732 Deogyeong-daero, Giheung-gu, Yongin-si, Gyeonggi-do 17104, Korea
(*Received 13 January 2021 • Revised 14 March 2021 • Accepted 4 April 2021*)

Table S1. Fitting parameters of the DSLF model

Parameters	$(HO)_2$BDC@CrN-12		MIL-101(Cr)-NH_2	
	CO_2	N_2	CO_2	N_2
q_1	8.453	0.931	1.079	1.865
k_1	6.3×10^{-3}	4.2×10^{-3}	9.6×10^{-4}	2.0×10^{-4}
n_1	0.525	2.884	0.980	1.080
q_2	15.09	1.91×10^{-3}	0.469	8.3×10^{-4}
k_2	2.22×10^{-3}	0.017	0.0592	0.3779
n_2	0.926	1.262	0.9221	1.12
R^2	0.9999	0.9997	0.9999	0.9996

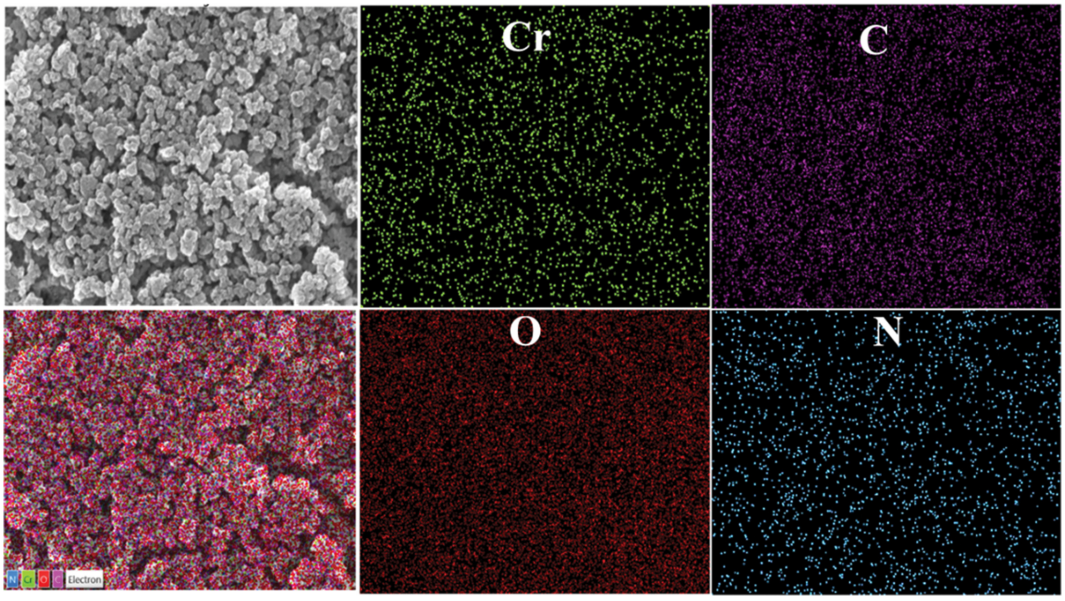

Fig. S1. EDX dot maps of Cr, O, C, and N on the prepared MIL-101(Cr)-NH_2.

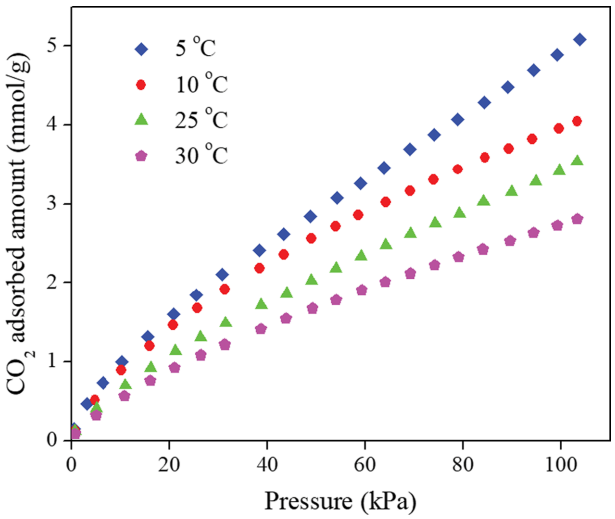

Fig. S2. CO_2 adsorption isotherms at different temperatures on $(HO)_2$ BDC@CrN-12.